THE DEVELOPMENT OF REDRAFT® SYSTEM IN BRAZILIAN PORTS FOR SAFE UNDERKEEL CLEARANCE COMPUTATION

by

Felipe Ruggeri[1], Rafael Watai[1], Guilherme Rosetti[1], Eduardo Tannuri[2], Kazuo Nishimoto[2]

[1]Argonautica Engineering & Research, Brazil

[2]University of São Paulo, Brazil

ABSTRACT

The increase of ship dimensions in the latest years combined to the requirements regarding the reduction of environmental impact during the maintenance dredging and economic constrains in the Brazilian ports require technological solutions in order to optimize the safe accessibility of large vessels. Most of these ports operate under a static draft rule regardless the environmental condition acting during the maneuver, which is theoretically a conservative approach. The bay close or restriction is usually performed based on experience, which may fail in the absence of objective parameters to define the adequate underkeel clerance, providing some unsafe situations mainly in the presence of misaligned wind and swell waves and/or negative meteorological tides. The development of computational resources, monitoring systems and communication technology in the last years provided the basis for integration of these tools into an automatic draft computation system, called as ReDRAFT, which integrates the environmental conditions collected in real-time to the hydrodynamic model of the port and ship dynamic model customized for each specific maneuver (ship properties, loading condition, inbound/outbond) in order to define the safe underkeel clearance for the maneuver. Moreover, the draft windows may be predicted based on the forecast models, which is also a powerful tool for planning. The numerical models allow more accurate predictions of the estuary environmental conditions, mainly waves, current and tide, which combined to the vessel numerical model can provide the ship motions in 6DoF. The ship motions on these large vessels are reduced for short period waves, thus allowing the increase the vessel draft. On the other hand, the vessel motions are significant for long waves, requiring the reduction of the vessel draft in order to mitigate the risk of bottom touch. The system is already operational in Santos and Rio de Janeiro ports, two of the most important ones in South America, for vessels considered as critical according to the nowadays port traffic. The PIANC Report n° 121 – 2014 factors are considered in the computation of the maximum safety draft. The ship related factors considered are the squat, dynamic heels due to turning and wind, wave response and net ukc. In order to simplify the utilization and avoid mistakes in the input data, a large database of vessels was created and summarized in a user-friendly interface, where the characteristics of each specific vessel is defined based on the IMO number, BZ code or vessel name. If a new vessel is operating in the port, the vessel is included in the software database using Lloyd's register information available in a standard "xml" format. The vessel hydrostatic/hydrodynamic characteristics are then interpolated using the software database if the dimensions are in the ranges of LOA, beam, depth and draft. The database contains the maximum wave motions of several points at the ship bottom considering a collection of wave periods, incidence direction, ship speed (encounter frequency correction), underkeel clearance, LOA, beam, depth, draft and ship type (tanker, bulk carrier or containership). The computations are performed in frequency domain using a higher order panel method based on spectral theory and a probabilistic approach. Since the ship geometry (stations) regarding each individual vessel is not available, some standard "design ships" are assumed and scaled to meet the desired LOA, beam, depth and draft, providing a NURBS (Non-uniform Rational Basis Spline) surface. The squat is computed based on literature regressions according to the Cb, ship speed (corrected to take into account the current effect) and channel geometry based on the database of hydrostatic properties, the pilots expertise regarding required ship speed to keep an adequate maneuverability and the channel bathymetry. The heel due to turning is computed according to the lateral wind, the metacentric height provided in the database and the wind measurements. The heel due to turning is computed using the ship speed and the turning radius computed from the channel alignment. The maneuvering margin (MM) is defined based on the pilots experience to guarantee the safety according to the environmental conditions, ship dimensions and available tugs. The system is already operational in Santos Port since 2015 and in Rio de Janeiro port since October 2016 for validation in order to provide reliability to the system.

INTRODUCTION AND MOTIVATION

The main Brazilian ports receive some of the largest vessels built in the last years to obtain gain of scale and reduce transportation costs related to export of oil, iron ore and other goods. The oil exploration has grown appreciably in the last years due to the discover of large oil reservoirs in the pre-salt layer in Santos Basin, requiring VLCCs (Very Large Crude Oil Carrier) to operate more often. A large project of iron ore exploration in the northeast region of Brazil and the increase of iron ore price motivates the increase of ULOC (Ultra Large Ore Carriers) maneuvers. The 366m containership class shall be operating in Brazilian ports in a near future, providing about 40,000 ton of additional displacement compared to the 333m class. These facts are also verified in (ANTAQ, 2015) (Brazilian Agency for waterway transportation) statistics, which show an average growth of 12.4% per year of cargo transportation since 2011 and a prediction of 150% growth in 2030 compared to 2012.
Beyond the large costs involved in the modification of the ports to receive these large vessels in a safety/efficient way, there is a large pressure from society for environmental sustainability in the new green world, see for instance, the several IMO regulations regarding ship efficiency, emissions and pollution. Each added tonnage during a vessel maneuver means an increase of ship efficiency by the increase of transport work, which is nowadays measured by EEOI (Energy Efficiency Operational Indicator) index defined by IMO (IMO - International Maritime Organization, 2009). A rule of thumb regarding the added transportation capacity considering an additional 10cm of operational draught can be seen in Figure 1.

$$EEOI = \frac{CO_2\ emissions}{Transported\ cargo\ \times distance} \qquad (1)$$

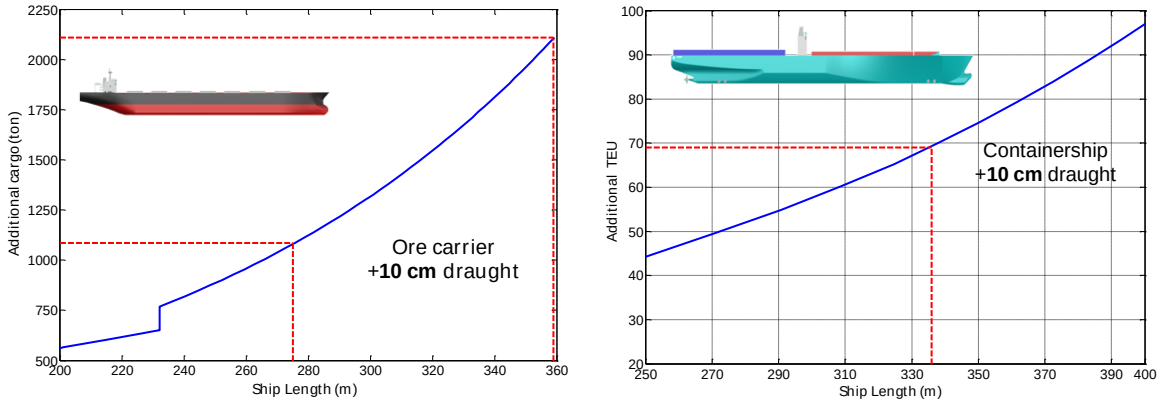

Figure 1 - Rule of thumb of added transportation capacity for 10 cm of added ship draught for ore carriers and containerships.

Moreover, navigation safety is a major concern during the maneuver of these large vessels, since the consequences are huge, requiring technological solutions to support these decisions.

The ReDRAFT® was developed to evaluate the maximum safety draught for navigation based on a scientific approach, combining almost real-time data measurements with the numerical model of the port and a digital model of each specific vessel, providing a customized draught rule for each maneuver. The system can also provide short and long-term forecasts of the maneuver window/maximum safety draught, the first one applied during the day-to-day ship planning and the second one for the maintenance dredging support decision. This digital twin of the port is one of the steps for the maritime 4.0 industry and it can be applied for several other applications, for instance, design of new terminals, evaluation of new vessels, queue studies, risk assessment, dredging optimization, environmental impact, oriented user database etc.

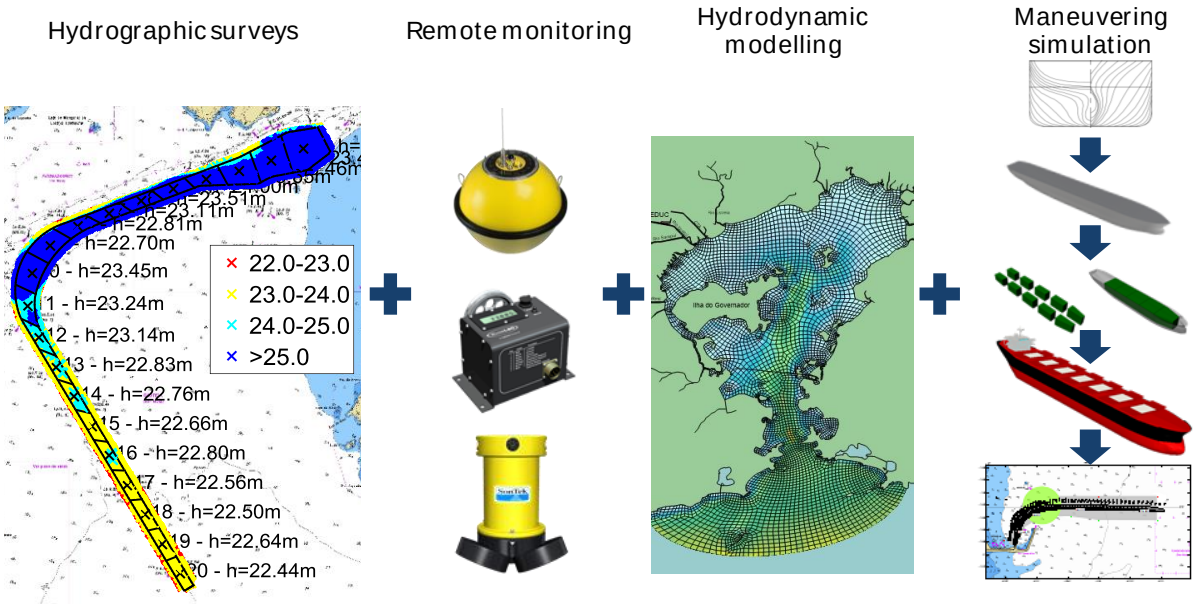

Figure 2 – ReDRAFT® Maritime Digital Twin

The definition of maximum safety draught is a challenge task due to the several variables involved, which may change in time and space according to the port specific conditions and the navigating ship. The traditional approach to this problem is to assume the environmental conditions as constant during the entire maneuver and take the channel depth as constant based on the lowest value, claimed as the channel depth. In some conditions the ship speed is also considered as constant during the entire maneuver to simplify the calculations, providing a single squat, wave motion, wind heeling etc, which is combined to a net underkeel clearance according to the bottom hardness.

Based on the predominant environmental conditions and pre-established operational limit in the design stage (directly related to the port downtime/efficiency assessment), a single safety margin for draught is usually defined in the Brazilian ports, regardless the day-to-day acting environmental condition during maneuver or ship type, as illustrated in Figure 3. This margin may lead to potential unsafe maneuvers if the environmental condition is beyond these pre-established values, requiring empirical expertise to avoid these risks, in some cases supported by using monitoring systems (wave buoys, adcp, tide gauges etc). However, in several complex conditions, e.g. multidirectional sea state condition and meteorological tides, the evaluation of ship interaction may be a challenge task.

On the other hand, in several conditions the draught may be increased without compromising the safety, improving cargo transportation efficiency, reducing the transportation cost and carbon footprint.

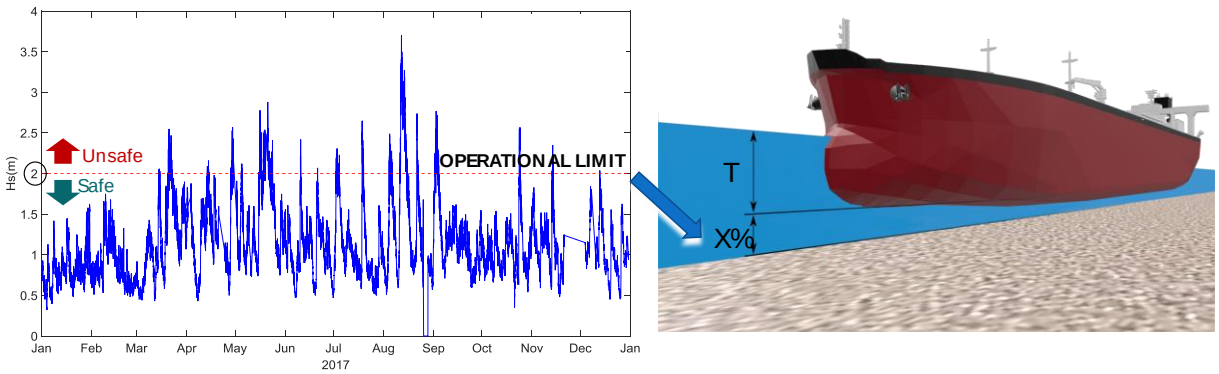

Figure 3 - Example of measured environmental condition and operational limit defined for the establishment of draft margin.

However, in several cases there are large variations in the channel depth, wave attenuation, current velocity, ship speed etc during the maneuvering, requiring an automatic tool to take in account all these aspects.

Moreover, several parts of the channel closer to the natural depth (routes to deep water) have softer bottoms compared to the regions closer to the berth, since the natural sand and muddy layers have not been modified yet, providing a spatially variable net underkeel clearance requirement.

A simplified comparison regarding wave energy propagation coefficients for 10 points in the access channel of an export port can be seen in Figure 4 considering the south and southwest incidence directions for 10s peak period spectrum. It can be verified the large attenuation of southwest condition compared to the south one, as the reduction of wave energy comparing point 1 (closer to the berth) to point 10 (in the outer region). These propagation coefficients shall change according to wave spectrum, wave frequency and offshore significant wave height, changing the vessel motions, therefore the required underkeel clearance for a safe navigation. The water level, channel depth, current, vessel speed and wind at each section of the channel will also change and influence in a different way at each section of the channel.

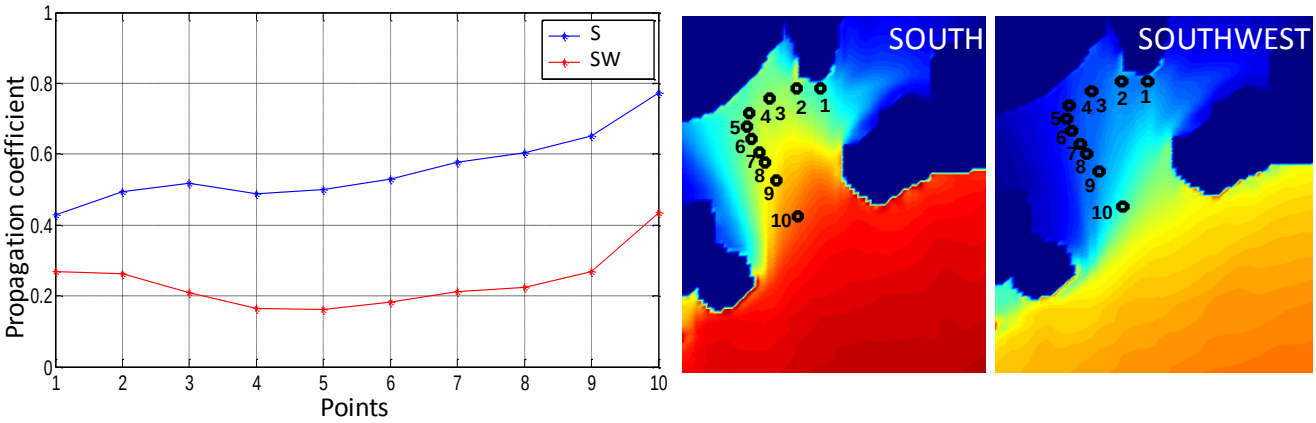

Figure 4 - Example of wave propagation coefficients for south and southwest incidence considering 10 points in the access channel of an export port for sea spectrum with peak period 10s.

The hydrographic surveys applied in the computations shall be in accordance with special class requirements defined in NORMAM 25, Brazilian navy standards, which is similar to S44 (International Hydrographic Organization, 2008) requirements from IHO (International Hydrographic Organization). The depths can be updated based on siltation maps computed using the validated hydrodynamic/wave propagation model to provide the bottom evolution, which is directly applied into the underkeel clearance assessment. An example of siltation map for an export port can be seen in Figure 5. The larger siltation is located closer to the coast (berth), while a smaller value is expected in the beginning of the access channel. The sinkage due to wave and squat are smaller closer to the berth since the ship speed is also smaller, as the wave incidence compared to the outer section. Based on that it can be expected different required depths in the channel, as different effects of siltation into the maneuver. The port digital model runs to provide the bottom evolution during the year, taking into account the winter and summer wave incidence, since harsh waves may modify accelerate the siltation/erosion appreciably of different parts of the channel.

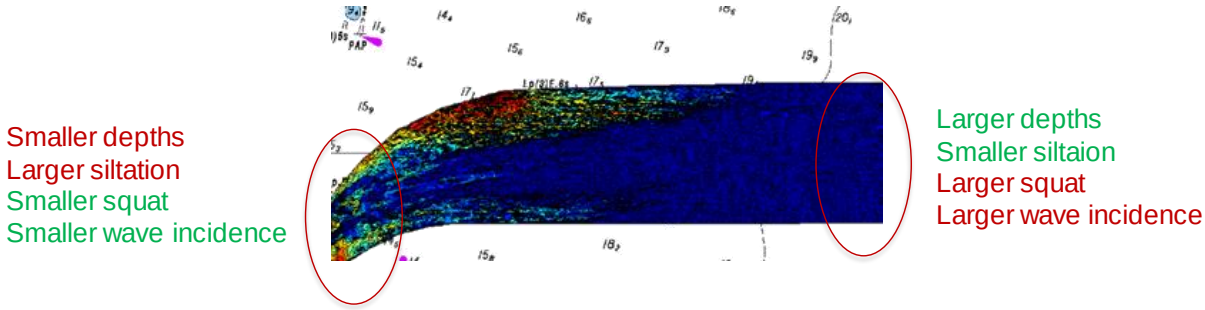

Figure 5 - Example of siltation map for an export port (blue color represents smaller siltation and red color a larger one).

SHIP MODELLING

The ship properties are defined based on large database of similar vessels, therefore for each one there is a specific digital model, containing the hydrostatic properties, hull geometry, panel meshes, loading conditions etc.

In some cases, the shipowner still has the lines plan of the ship, allowing an even more accurate digital model. If the lines plan is not available, the appropriate benchmark hull may be scaled and changed by Lackenby transform (Lackenby, 1950) to achieve the desired hydrostatic properties. Some examples of benchmark containership may be seen in Figure 6.

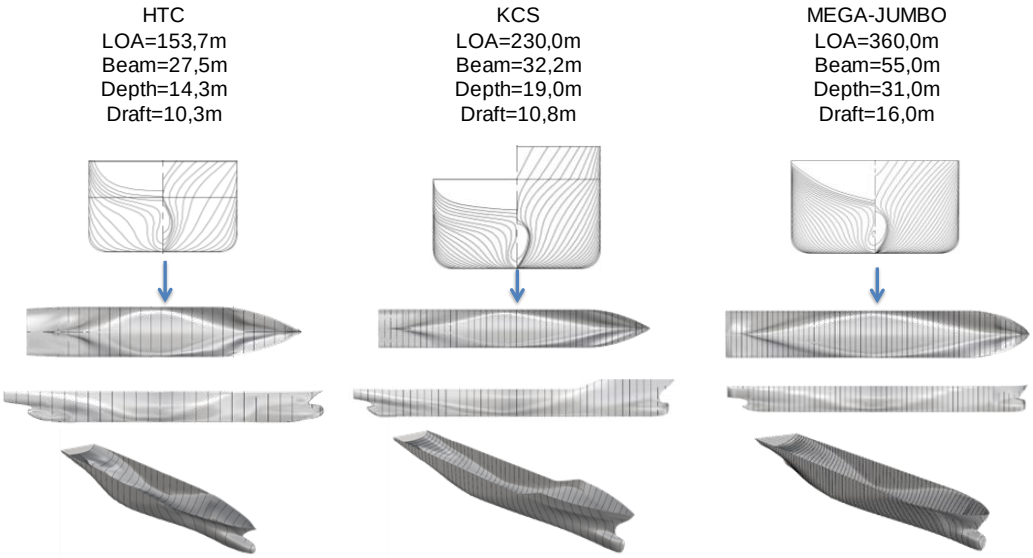

Figure 6 - Examples of benchmark containerships.

The ship geometry is generated using NURBS (Non-uniform Basis Spline), one of the standards formats applied in CAD industry, which is applied in the hydrostatic properties, wave response and squat assessment, as described next. The NURBS surface is described considering several patches, each one described based on *(2)*, where p is the degree of the spline, $N_{i,p}$ is the basis function, $\vec{C}_{ij}$ are the control points, w_{ij} are the control points weights and u, v is the unitary surface domain. This approach allows a simple, efficiency and robust way to store the hull surface. Moreover, the surface is continuous, therefore the normal vector and Jacobian are also continuous, which will be important in the seakeeping computations due to a continuous potential function, as discussed later. More details may be found in (Ruggeri, et al., 2018) and (Ruggeri, 2016).

$$\begin{Bmatrix} x(u,v) \\ y(u,v) \\ z(u,v) \end{Bmatrix} = S(u,v) = \frac{\sum_{i=1}^{N_u}\sum_{j=1}^{N_v} w_{ij}\vec{C}_{ij}N_{i,p}(u)N_{j,p}(v)}{\sum_{i=1}^{N_u}\sum_{j=1}^{N_v} w_{ij}N_{i,p}(u)N_{j,p}(v)}, 0 \le u \le 1, \qquad 0 \le v \le 1 \tag{2}$$

The ship digital model also considers the cargo and ballast tanks to obtain the cargo distribution and free surface effect more accurately, as illustrated in Figure 7. The loading condition is evaluated based on the general arrangement, capacity plan and trim& stability booklet.

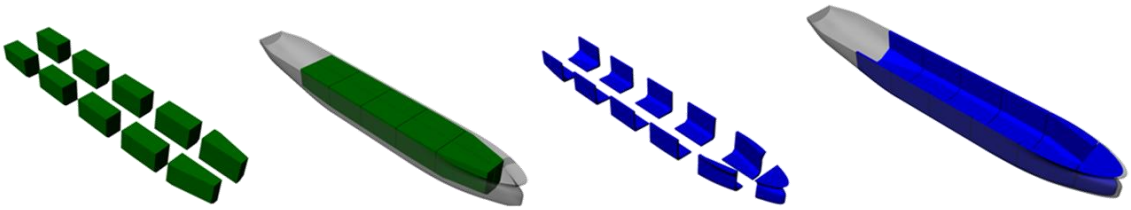

Figure 7 - Example of digital model of a crude oil carrier considering the cargo (left) and ballast (right) tanks highlighted applied for moment of inertia and vertical center of gravity calculation.

The vertical center of gravity is evaluated based on (3), where $\mathrm{VCG_{light}}$ is the vertical center of gravity of the lightship, $\mathrm{W_{light}}$ is the lightship weight, $\mathrm{VCG_{i,cargo}}$/$\mathrm{VCG_{i,ballast}}$ are the center of gravity of the several cargo/ballast tanks (or containers) and $\mathrm{W_{i,cargo}}$/ $\mathrm{W_{i,ballast}}$ are the weight of each specific item. The center of gravity may also be provided by ship master based on the planned load, if the data is provided.

$$VCG = \frac{\left(VCG_{light}W_{light} + \sum_{i=1}^{N_c} VCG_{i,cargo}W_{i,cargo} + \sum_{i=1}^{N_b} VCG_{i,ballast}W_{i,ballast}\right)}{W_{light} + \sum_{i=1}^{N_c} W_{i,cargo} + \sum_{i=1}^{N_b} W_{i,ballast}} \quad (3)$$

The moment of inertia in x direction (surge) is evaluated using Steiner's theorem given in (4), where $\mathrm{I_{xx,LS}}$, $\mathrm{I_{xxi,cargo}}$ and $\mathrm{I_{xxi,ballast}}$ are the moments of inertia regarding the lightship, cargo and ballast tanks computed considering the principal axes, $\mathrm{W_{i,cargo}}$/$\mathrm{W_{i,ballast}}$ are the cargo/ballast weights, $(\mathrm{x_{Gi,cargo}}, \mathrm{y_{Gi,cargo}}, \mathrm{z_{Gi,cargo}})$/ $(\mathrm{x_{Gi,ballast}}, \mathrm{y_{Gi,ballast}}, \mathrm{z_{Gi,ballast}})$ are the cargo/ballast centers of gravity and $(\mathrm{x}_{CG}, y_{CG}, VCG)$ the ship center of gravity coordinates considering a coordinate system located in the baseline amidship.

$$I_{xx} = I_{xx,LS} + \sum_{i=1}^{N_c} \left\{ I_{xxi,cargo} + W_{i,cargo}\left[\left(y_{Gi,cargo} - y_{CG}\right)^2 + \left(z_{Gi,cargo} - VCG\right)^2\right]\right\} + \sum_{i=1}^{N_b} I_{xxi,ballast} + W_{i,ballast}\left[\left(y_{Gi,ballast} - y_{CG}\right)^2 + \left(z_{Gi,ballast} - VCG\right)^2\right] \quad (4)$$

Since the computation of the lightship moment of inertia taken into account each structural stiffener and the variation of plate thickness along the entire ship would be very difficult due to the huge number of details, see for instance Figure 8, an equivalent thickness is defined ($t_{eq} = W_{light}/S_{total}$) taking into account the ship plating without these elements.

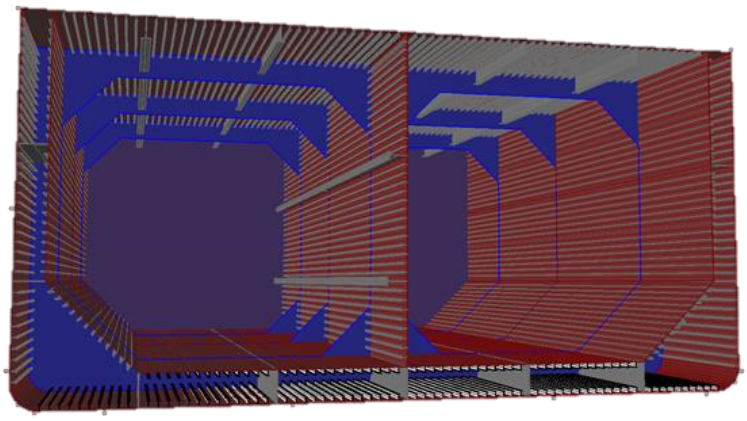

Figure 8 - Example of structural section considering the all stiffener elements of a real tanker.

The lightship moment of inertia in x direction is then computed using (5), considering only the plates. The moments of inertia in other directions are computed analogously.

$$I_{xx,LS} = t_{eq} \iint_{S_{total}} \left[\left(z - VCG_{light}\right)^2 + y^2\right] dS \quad (5)$$

The 6x6 hydrostatic restoration matrix is computed using Gauss theorem in the submerged hull surface considering the appropriate vector field combined to center of gravity position, as demonstrated in

(WAMIT Inc, 2015), (Ruggeri, 2012) and (Ruggeri, 2016). The linear free surface effect corrections are also taken into account for loaded tanks within 5% to 95% of the nominal capacity.

If the detailed loading condition is not available, some variations of cargo loading are performed to obtain the mean draft, trim and list following the stability requirements from IMO (IMO - International Maritime Organization, 2008) and maximum allowed bending moment and shear stress. These combinations are usually limited for bulk carriers and tankers but quite more complex for containerships due to the several possibilities of cargo allocation and container weight, see for instance in Figure 9.

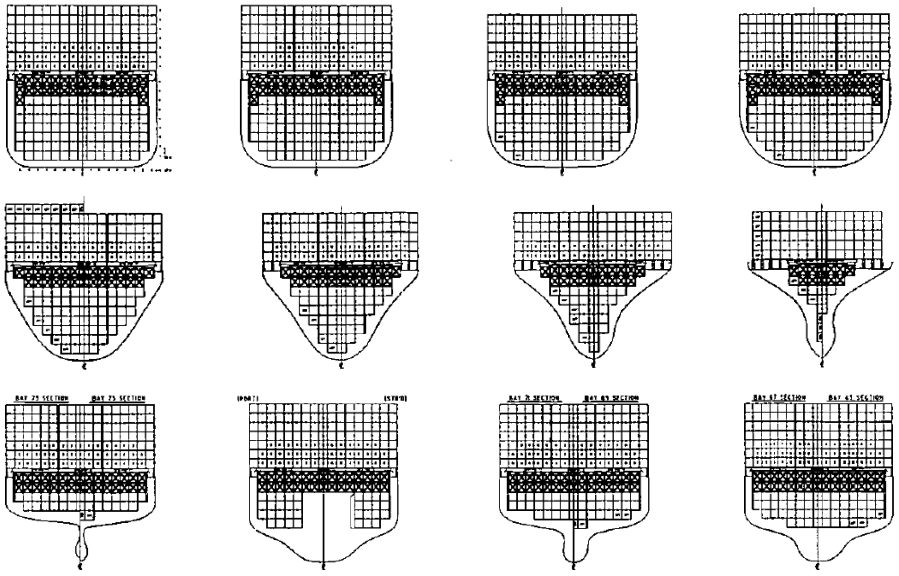

Figure 9 - Example of 366m containtership section.

The metacentric height and moments of inertia are compared to reference values, for example (Journée, et al., 2011), (Schneekluth, et al., 1998), (Yilmaz, et al., 2001) and (PIANC, 2014), to verify the coherence of the data. The flat bottom, propeller, rudder and bulb are discretized considering several points based on the 3D model of each specific ship. There are significant differences between a bluff ship (e.g. large bulk /crude oil carrier) and slender one (e.g. container ship, LNG carriers etc.) due to the different hull lines and block coefficient, as illustrated in Figure 10.

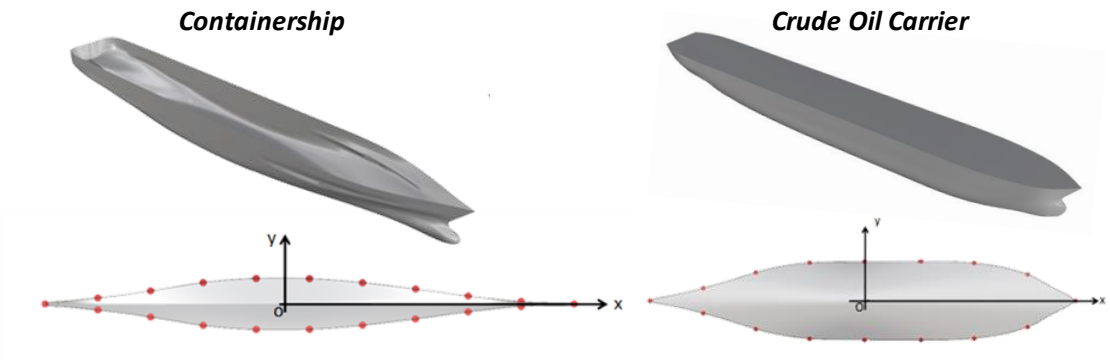

Figure 10 - Critical points in the flat bottom of a containership (left) and a crude oil tanker (right).

A pre-defined database is built for the several ship types based on fleet study and regressions, see for instance, (Kristensen, 2012) and (Kristensen, 2013). In the operational tool this data is automatically obtained from class societies database according to IMO number. It shall be noticed that following this approach the ship is no longer only a simple combination of LOA, Beam and DWT, which is usually considered in the simplified safety margin computation. Instead the ship now has a complete detailed digital model applied during the computations.

SHIP SPEED

The ship speed during the several sections of the channel can be suggested during the maneuver to reduce the risk of bottom touch. However, there are limits related to the maneuverability margin (MM) that cannot be exceed, which are evaluated in a real-time simulation campaign. One of the main references is the TPN Simulator, developed by University of São Paulo, Petrobras and Transpetro with the technical collaboration of the Brazilian Pilots Association (CONAPRA) (Tannuri, et al., 2014).

If the ship already operates in the port with a constrained draught under static rules a first guess of the ship velocities in the several sections can be obtained based on track records of past maneuvers, as the drift angles, which may be combined to current speed, water level, wind etc to obtain a better comprehension of these limits. The pilots' expertise provides additional insights regarding the key aspects of the maneuver and points of additional attention during the studies.

An example of ship speed distribution along the channel section can be seen in Figure 11, where each dot is an observed maneuver, with section 1 closer to the seaside and section 99 closer to the turning basin/berth basin. Based on these records, the speed statistical distribution for each section can be created, as the probability of exceedance.

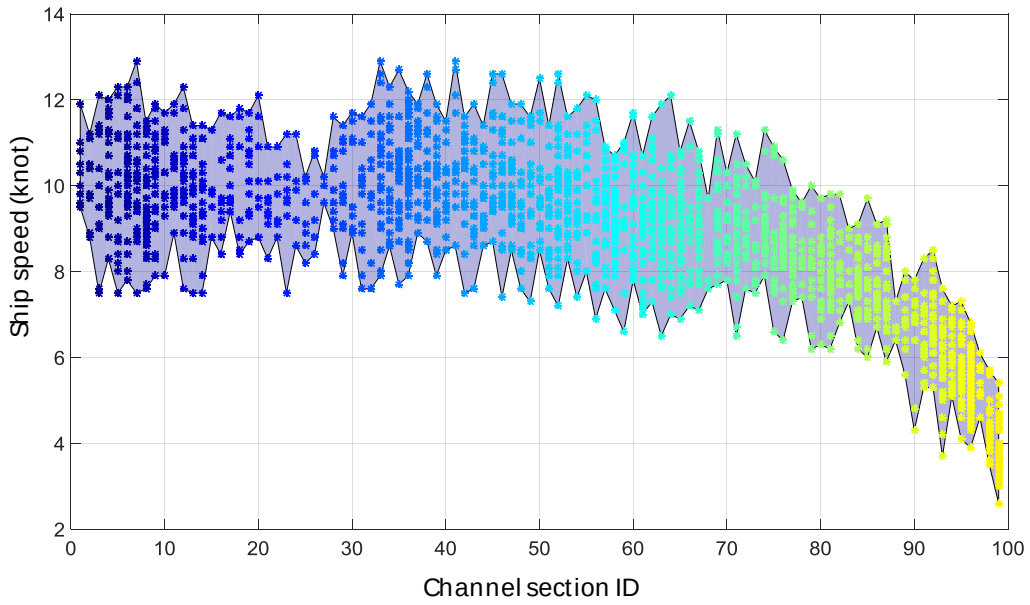

Figure 11 – Example of ship speed records along the channel sections considering several observed maneuvers.

SQUAT

The squat may be computed following several different techniques, from simplified regression formulas to customized model tests and state-of-art higher order panel mesh using the "real" bathymetric surveys combined to the tide level and current values. An example of panel mesh applied for squat computation considering a real bathymetric survey can be seen in Figure 12. It shall be noticed that even this method has some limitations inherent to potential flow theory.

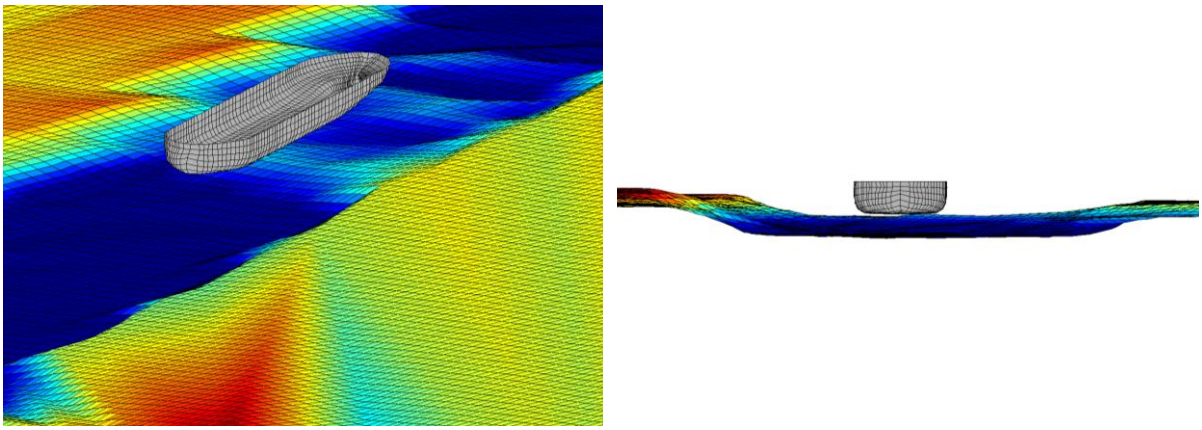

Figure 12 - Example of panel mesh considering a specific ship and the bathymetric survey.

In the 10 last years the CFD (Computational Fluid Dynamics) techniques based on FVM (Finite Volume Meshes) and FEM (Finite Elements Method) have evolved appreciably in terms of computational efficiency and mesh generation capability to represent the real seabed in the computations. However, the time required does not allow the application for an operational tool and the convergence process still not robust enough without an expert supervision.

The regression formula proposed by Huuska (Huuska, 1976) still the most accepted approach, which is applied section by section according to the ship speed (discussed earlier) considering the current effect (relative velocity) and the blockage correction K_{Si}, which defines the unrestricted, restricted and channel conditions. The squat value can be computed according to (6), where C_S is an adjustment coefficient based on block coefficient, L_{pp} is the length between perpendiculars and F_{nhi} is the Froude number based on the mean water depth and tide level. The same channel may have different configurations according to the blockage effects, see for instance Figure 13 considering several sections of the same channel.

$$\Delta z_{squat,i} = C_S \frac{\nabla}{L_{pp}^2} \frac{F_{nhi}^2}{\sqrt{1 - F_{nhi}^2}} K_{Si} \tag{6}$$

$$C_S = \begin{cases} 1.7, if\ C_B < 0.70 \\ 2.0, if\ 0.70 < C_B < 0.80 \\ 2.4, if\ C_B > 0.80 \end{cases} \tag{7}$$

$$F_{nhi} = \frac{V_{shipi} + V_{corr}\, cos(\theta_{curr} - \theta_{ship})}{\sqrt{g(h_{Mi} + m_i)}} \tag{8}$$

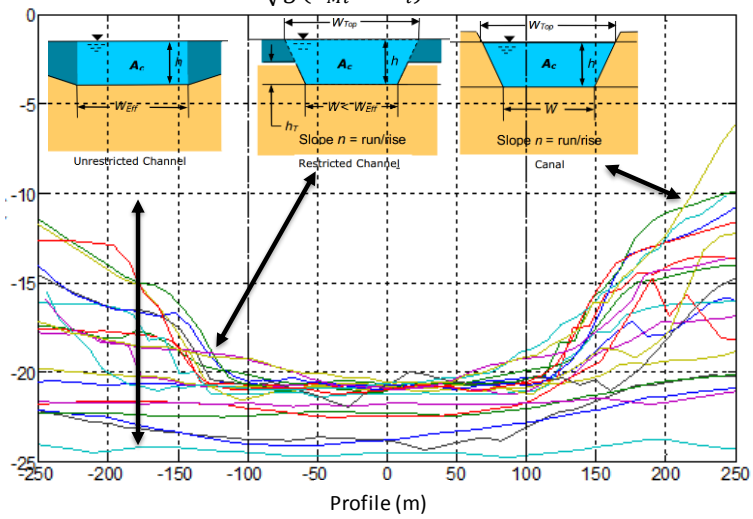

Figure 13 – Example of several section profile in the same access channel (each line is a specific section).

WIND HEELING

The sinkage due to wind heeling is computed based on *(9)*, where θ_{Wi} is the heeling angle at section i and x_p is the x-coordinate of each point p located at the ship bottom, as described previously. The wind heeling angle is obtained based on ship stability *(10)*, where M_{Wi} is the wind heeling moment, ρ_W is the salt water density and GM_T is the transversal metacentric height. The metacentric height is also obtained based on the ship modelling procedure described earlier.

$$\Delta z_{wind,pi} = x_p sin(\theta_{Wi}) \quad (9)$$

$$sin(\theta_{Wi}) = \frac{M_{wi}}{\rho_W g \nabla G M_T} \quad (10)$$

The wind heeling moment is computed applying *(11)* following (PIANC, 2014), where ρ_{air} is the air density, A_L is the projected lateral windage area, $V_{WR}i$ is the relative wind velocity in section I and C_{Wy} the transversal wind force coefficient, computed by *(12)*, where C_{Ynk} are coefficients obtained from tables provided in (Yamano, et al., 1197), A_F is the frontal area, B is the beam and x_L is the distance between the forward perpendicular and the center of projected area, computed using the general arrangement draw, see for instance Figure 14.

$$M_{Wi} = \frac{1}{2}\rho_{air} C_{wy} A_L V_{WRi}^2 \left(KG - \frac{T}{2}\right) \quad (11)$$

$$C_{wy} = \sum_{n=1}^{3}\left[\left(C_{Yn0} + C_{Yn1}\frac{A_{V,L}}{L_{pp}^2} + C_{Yn2}\frac{x_L}{L_{pp}} + C_{Yn3}\frac{L_{pp}}{B} + C_{Yn4}\frac{A_L}{A_F}\right) sin(n\theta_{WRi})\right] \quad (12)$$

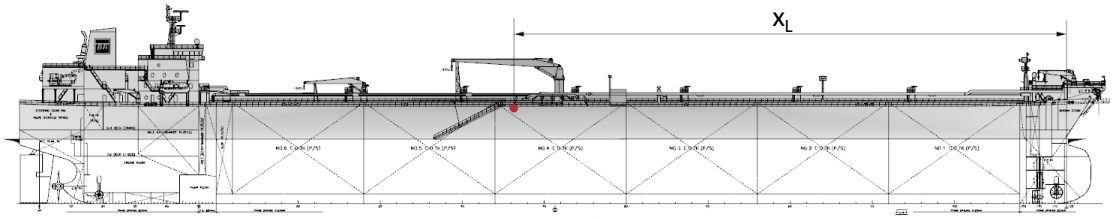

Figure 14 - Example of general arrangement used for x_L computation.

It should be noticed that several other references are available in the literature, see for instance (Isherwood, 1972), (Blendermann, 1994) and (Lindeen, 2008) for container ships coefficients. The application of CFD may be performed, as wind tunnel tests, to obtained the wind coefficients, mainly for new vessels without data available. The advantage of CFD simulations is the possibility to compute in both model and full scale taken into account the scale effects accurately.

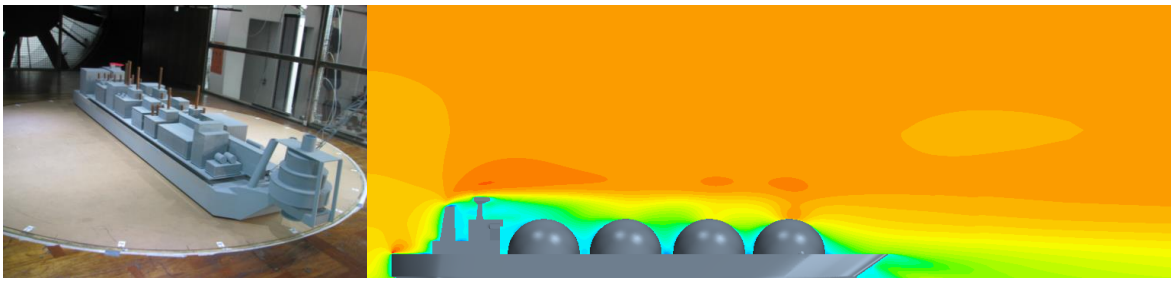

Figure 15 - Example wind tunnel test (left) for a FLNG and CFD simulation (right) considering the velocity field around a LNG Carrier.

The wind areas stored are in the ship modelling are defined in the design draft condition, therefore these values shall be corrected for other drafts based on *(13)*, where T_{des} is the design draft.

$$A_F(T) = A_F(T_{des}) + (T_{des} - T)B,\ A_L(T) = A_L(T_{des}) + (T_{des} - T)L_{pp} \quad (13)$$

The sinkage due to wind action in the longitudinal direction is required since the longitudinal metacentric height is in the order 100 times the transversal metacentric height. Moreover the frontal wind area is usually appreciably smaller than the transversal one.

DYNAMIC HEELING

The dynamic heeling angle is computed using *(14)* according to (PIANC, 2014), where V_{SRi} is the relative ship speed taken into account current effects in section i, l_R is the heeling lever *(15)* and R_C is the turning radius, computed from the nautical chart at each section. The additional sinkage due to the dynamic heeling is then computed applying *(16)*. The turning radius is defined as the minimum value at each section and for straight ones the value tends to infinity therefore the heeling angle tends to zero. An example of the outer curve in the access channel of Santos port is shown in Figure 16.

$$\phi_{Ci} = \frac{l_R V_{SRi}^2}{g R_C GM} \tag{14}$$

$$l_R = VCG - \frac{T}{2} \tag{15}$$

$$\Delta z_{dyn,pi} = x_p \, sin(\phi_{Ci}) \tag{16}$$

Figure 16 - Example of outer curve in the access channel of Santos port.

WAVE RESPONSE ASSESSMENT

The wave response is evaluated in frequency domain based on the ship RAO (Response Amplitude Operators) of each specific ship during the maneuver. The potential flow theory is applied (Newman, 1977), (Faltinsen, 1990), (Bertram, 2000), (Mei, et al., 2005) using a higher order panel method based on the NURBS surface presented earlier for the geometric description and B-spline description regarding the potential function, therefore velocity field and other quantities. The double-flow linearization is applied for low ship speeds/depth Froude numbers ($F_{nh} < 0.3$). An example of panel mesh can be seen in Figure 17 considering the b-spline potential subdivision and the normal vectors in the center of the higher order panels.

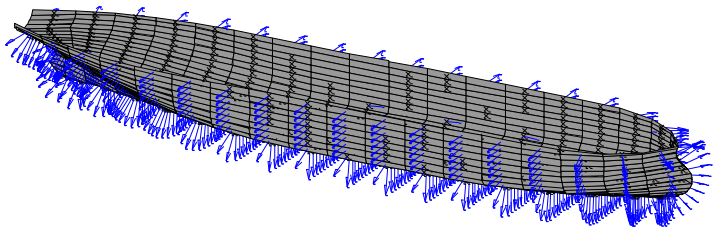

Figure 17 - Example of panel mesh and normal vectors for a tanker.

The basis flow is solved using the Green function considering the Rankine source mirror technique to guarantee the no-flux condition in the bottom and mean free surface, illustrated in Figure 18. Since the no-flux condition is considered in the bottom and mean free surface, an infinite number of images shall be applied. The mean hydrodynamic depth is applied as reference depth applying the algorithms proposed by (Newman, 1992), (Breit, 1991) for the series evaluation since the convergence is low for reduced underkeel clearances.

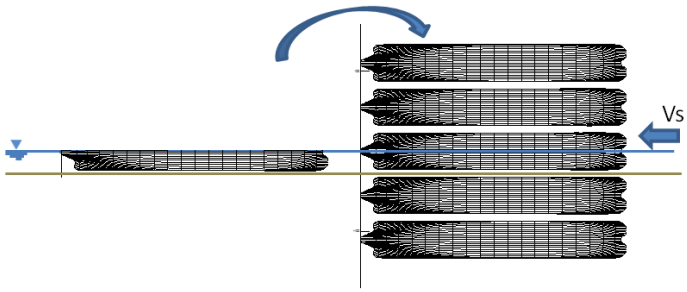

Figure 18 - Source mirror technique for basis flow computation.

The widely known transient Green function (Wehausen, et al., 1960) is applied for the wave-body interaction during the first order radiation and diffraction potential computations, as shown in (17). The evaluation of the Green function is performed using the auto-function expansion proposed by (John, 1949) combined to the algorithms presented in (Li, 2001), (Newman, 1985), (Liu, et al., 2015) and (Guha, et al., 2016) according to the ratio R/h ($R = \sqrt{(x_i - x_j)^2 + (y_i - y_j)^2}$ and h the mean water depth).

$$G_{ij} = \frac{1}{r_{ij}} + \frac{1}{r_{ij}'} + 2PV \int_0^\infty \frac{(\mu + K)\, exp(-\mu h)\, exp(-\mu h)\, cosh\left(\mu(z_j + h)\right) cosh\left(\mu(z_i + h)\right)}{\mu\, sinh(\mu h) - K cosh(\mu h)} J_0(\mu R) d\mu \qquad (17)$$

$$+ \frac{i2\pi(k + K)\, exp(-kh)\, sinh(kh)\, cosh\left(k(z_j + h)\right) cosh\left(k(z_i + H)\right)}{Kh - sinh^2(kh)} J_0(kR)$$

The solution of the so-called radiation and diffraction problems together with the basis flow potential solution provides the added mass, wave damping and excitation forces acting in the ship for each specific regular wave. The RAOs are obtained applying *(18)*, where $\omega_e = \omega - kV_s \cos\theta$ is the encounter frequency (ω is the wave frequency, V_s is the vessel speed, k the wave number and θ the wave direction, [M] is the generalized physical mass matrix, [A] are the added mass matrix, [C] is the external damping, [B] the potential damping, [K] the hydrostatic stiffness matrix, $\{F^{(1)}\}$ is the generalized excitation force vector and $\{X\}$ is the RAO in 6 degrees of freedom.

$$\{-\omega_e^2([M] + [A]) + i\omega_e([C] + [B]) + [K]\}\{X\} = \{F^{(1)}\} \qquad (18)$$

The validation of the RAOs are performed in model scale in wave basins or towing tanks following the International Towing Tank Conference (ITTC) guidelines, some examples are the active absorption wave basin of the Numerical Offshore Tank and IPT towing tank in Brazil. A comparison between numerical and experimental RAOs obtained for several wave frequency and wave directions, without forward speed, can be seen in Figure 19 for a large tanker considering the heave degree of freedom. The points in the figure are the experimental measurements including an error bar while the continuous lines are the numerical computations. The wave incidence orientation is 0º for following seas, 90º for beam seas starboard and 180º for head seas.

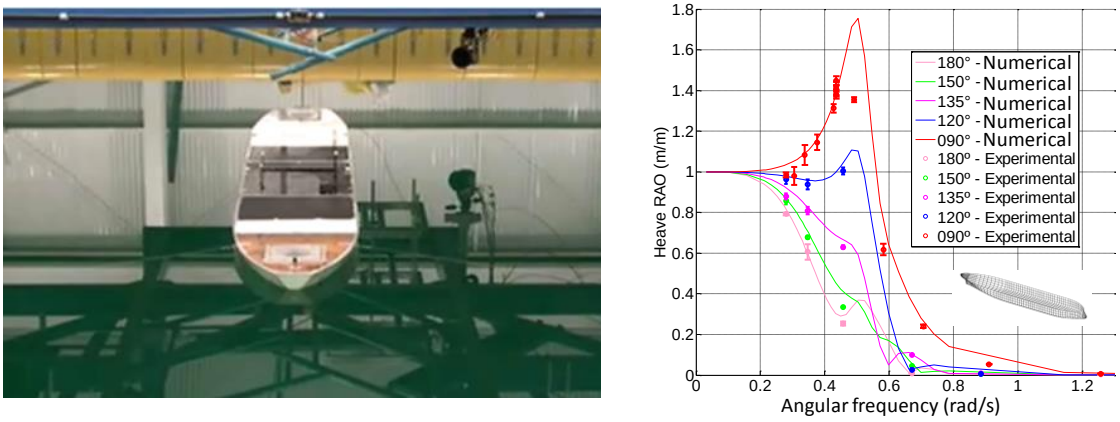

Figure 19 - Example of RAO comparison considering wave basin test and numerical computation for a large tanker.

Since in the potential theory the viscous damping effects are neglected an external damping shall be included, mainly in the roll degree of freedom to provide more realistic results. Several studies have been performed in the last 40 years to provide a consistent approach to compute this effect, see for instance (Ikeda, et al., 1976), (Ikeda, et al., 1977), (Ikeda, et al., 1977), (Ikeda, et al., 1978), (Himeno, 1981) and (Ikeda, 1982). The roll damping prediction in harsh environmental conditions and irregular sea states still a challenge, which is even more complex in shallow waters due to the small gap between the ship and seabed, that affects the vortex shedding pattern. An illustration of vorticity for several roll amplitudes of a crude oil carrier in deep water can be seen in Figure 20, where it can be verified the difference in vorticity pattern. In the absence of measured data or Ikeda's prediction method a conservative 5% critical damping may be considered.

5º 7º 10º

Figure 20 - Example of the vorticity field in the roll motion of a crude oil carrier under regular waves for several roll angles.

The heave, roll and pitch motions are combined to provide the vertical motion of each point presented earlier using (19), where (x_p, y_p) are the coordinates of each point and $X_k(\omega, \theta, V_s)$ (k=3,4,5) are the complex RAOs.

$$RAO_{zp}(\omega, \theta, V_s) = X_3(\omega, \theta, V_s) + X_4(\omega, \theta, V_s)\left(y_p - y_{CG}\right) - X_5(\omega, \theta, V_s)\left(x_p - x_{CG}\right) \qquad (19)$$

The ship responses are evaluated based on the spectral moments computed for each sea-state in the several sections of the access channel according to (20), where $S_{\zeta i}(\omega_e, \theta)$ is the directional sea spectrum at section i.

$$m_{npi}(V_s) = \int_0^{\infty} \int_0^{2\pi} \omega_e^n(\omega, \theta, V_s) \left| RAO_{zp}(\omega, \theta, V_s) \right|^2 S_{\zeta i}(\omega, \theta, V_s) d\theta d\omega \qquad (20)$$

The directional sea spectrum measured using the wave buoy is transferred using up to 27 bins or using the Fourier coefficients of energy distribution in terms of direction for each wave frequency. Due to the inherent multidirectional sea state conditions generated offshore, several ports in Brazil are exposed to multidirectional sea state conditions, mainly the ones outside bays. The sea spectrum changes in shallow water due to the bottom friction, refraction and other effects, acting differently according to the frequency and direction.

An example of this phenomenon is illustrated in Figure 21 for an exposed port in Brazil, where it can be verified that in the outer section of the access channel there are two different main sea components from east and south, while in the middle section the energy from south has been almost dissipated.

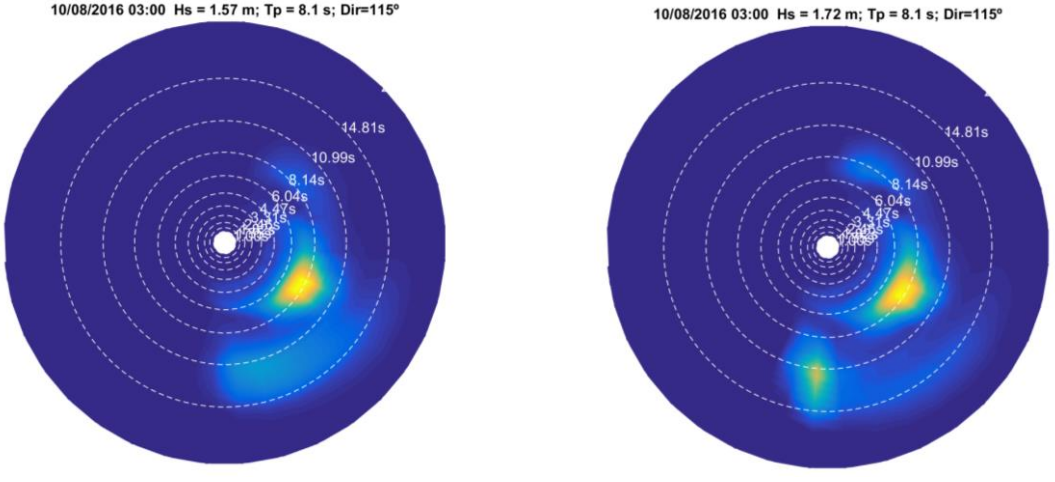

Middle section Outer section

Figure 21 - Example of sea spectrum in the outer section and middle section of an access channel.

The complex nature of the Brazilian coast does not allow a simple parametric sea spectrum based only on significant wave height, peak period, wave direction and spread factor to describe the wave energy distribution properly in several locations. In several cases the parametric sea spectrum approach may identify a higher peak period due to wind influence or some wave components, neglecting wave energy in low wave frequencies (high periods).

An example of comparison regarding significant wave height and peak period for a port located in the northeast region of Brazil, considering the measured data (with a single peak period output) and numerical results regarding the two main partitions of the directional sea spectrum obtained using a watershed technique can be seen in Figure 22. It can be verified that according to the energy distribution (significant wave height) the wave buoys output alternates between the first and second partitions peak period identification, although there are no appreciably modifications in the sea state. In fact, when the second partition is not present anymore the wave buoy measurement and numerical simulation identify the same peak period with a good accuracy. The analysis of one year of wave data provides that about 85% of the records contain more than one partition.

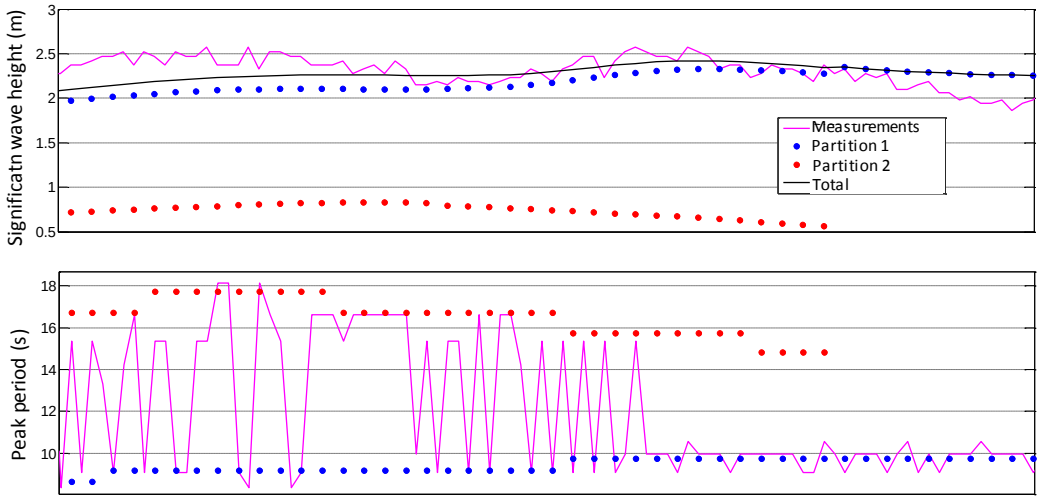

Figure 22 – Example of significant wave height and peak period measured with a wave buoy with a single peak period output and the numerical simulations for a port located in the northeast region of Brazil.

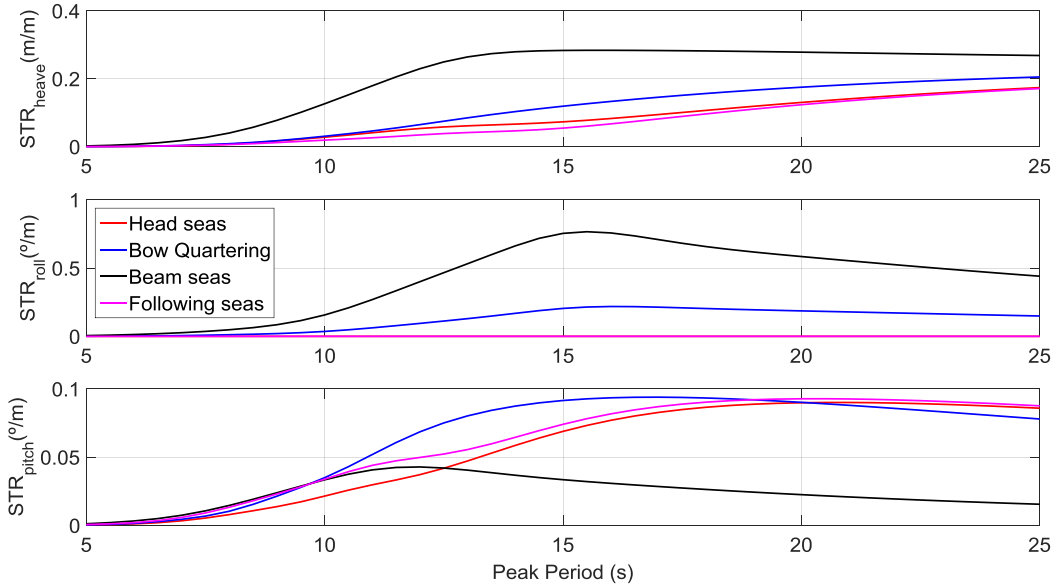

Figure 23 - Example of numerical computation of Short-term responses (STR) for several peak periods of a Very Large Ore Carrier at 8 knots under several wave incidences for standard Jonswap sea spectrums.

However, since large vessels are susceptible only to wave energy in higher periods, a simplified sea spectrum description would provide unsafe vessel motion predictions when identifying the lower peak period, motivating the use of the full directional sea spectrum in the vessel motions prediction. The short term responses regarding heave, roll and pitch motions for several peak periods and wave incidences computed numerically for a very large ore carrier at 8 knots of forward speed can be seen in Figure 23, where the variation of vessel responses according to peak period may be verified, as the influence of wave direction.

The measured data is extrapolated to the other sections of the channel based on the numerical propagation model after the appropriate calibration and validation procedure. The application of ANN (Artificial Neural Network) technique for energy adjustment in the sea spectrum is applied to improve the wave condition extrapolation and forecast more accurately.

The sea spectrum is transformed from the fixed reference to the ship one based on the encounter frequency spectrum as proposed in (Lewis, 1988). Some modification shall be performed to include the shallow water effect, as shown in *(21)*, with the dispersion relation for shallow water given in (22). The derivative of wave number according to wave frequency is evaluated using the implicit differentiation method.

Since the computations are performed considering the directional sea spectrum, for each wave frequency and wave direction a different encounter frequency is obtained, which shall be considered very carefully from the computational point of view, mainly under following sea condition, where there is not an unique solution between the wave frequency and encounter frequency.

$$S_\zeta(\omega,\theta,V_s) = \frac{S_\zeta^*(\omega,\theta)}{\left|1-\frac{dk}{d\omega}V_s\,cos\,\theta\right|} \quad (21)$$

$$\frac{\omega^2}{g} = k\,tanh(kh) \quad (22)$$

The maximum motion of each point located in the ship bottom is computed using (23) assuming the vessel motions as a Gaussian process, thus the amplitude of the motion as a Rayleigh distributions (Ochi, 1998). The bandwidth factor $\epsilon = \sqrt{1-\frac{m_{2pi}^2}{m_{0pi}m_{4pi}}}$, t is the exposed time and the period between ascendant zeros is $T_{zp} = 2\pi\sqrt{\frac{m_{0pi}}{m_{2pi}}}$.

$$\Delta z_{wave,pi} = 2\sqrt{m_{0pi}}\sqrt{\frac{1}{2}ln\left(\frac{2\sqrt{1-\epsilon^2}}{1+\sqrt{1-\epsilon^2}}\frac{t}{T_{zpi}}\right)} \quad (23)$$

The maximum vertical motion is combined to the probability of bottom touch to obtain the maximum safety draft for the maneuver.

INTEGRATION OF THE VARIABLES

In the forecast model the wave, current, wind and tide level predictions at each section of the channel are applied into the prediction of the underkeel clearance or maximum safety draft for the maneuver. If the tide window shall be predicted for a pre-established draft the computation is simpler because the ship model is invariable. On the hand, for the maximum safety draft prediction, the ship modelling shall change according to different possible loading conditions.

Regardless the analysis performed there is always an error between the predicted environmental condition and the “real” condition acting during the maneuver since there are several complex phenomena to be modelled. Although the best efforts are made during the calibration process and a good precision may be achieved, the accuracy of some extreme meteorological tides or harsh wave conditions may be a problem. Moreover, there is a lag between the measured data received and the “actual” environmental condition during the maneuver. In order to handle this fact, some allowances

curves are created based on the data applied during the validation phase of the hydrodynamic/wave propagation model in order to evaluate the probability that the environmental conditions is different of the predicted one.

An example of the difference between the numerical prediction of significant wave height and the measured one can be seen in Figure 24. This probability curve is discretized in several different ranges and for each one the probability of bottom touch is evaluated. The same procedure is performed for ship velocity and water level prediction, the former based on ship velocity records presented earlier for the several sections of the channel.

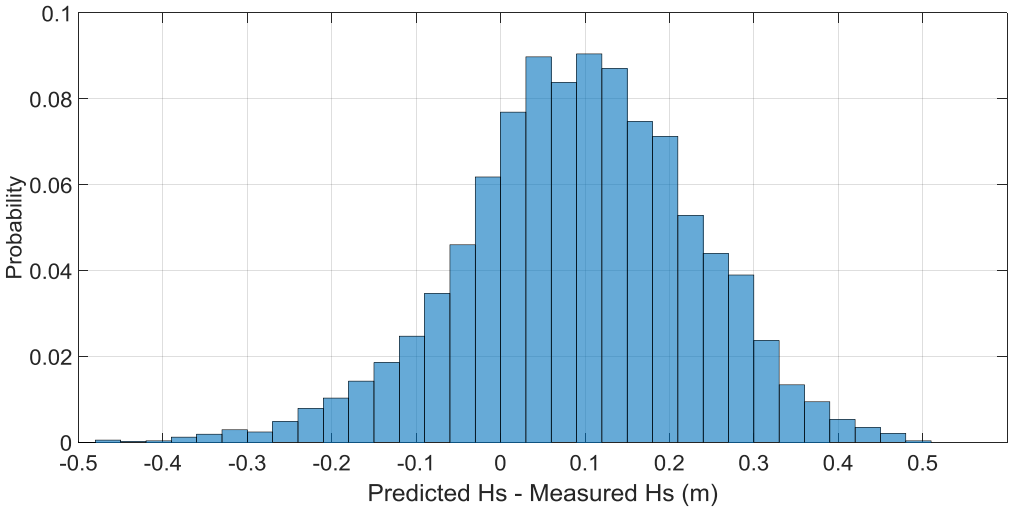

Figure 24 - Example of error probability distribution of the difference between the predicted significant wave height and the measured one.

The net ukc is defined according to (PIANC, 1985), as what is left after the summation of the several effects presented earlier, and it is computed based on (24).

$$net\ ukc_{i,p} = h_i + \Delta h_i - \Delta z_{wind,pi} - \Delta z_{dyn,pi} - \Delta z_{wave,pi} \qquad (24)$$

Since several quantities are changing during the maneuver the probability of bottom touch is computed using ***(25)***, which is the complement probability of the no bottom touch probability in any section of the channel, where Δt_i is the time of navigation in section i and $P\left(net\ ukc_{i,p} \leq 0\right)$ is the probability of bottom touch of the point p in section i of the channel, which is equal to the probability that the wave response to exceed the net ukc under a specific water level, ship speed and wave condition times the probability of cooccurrence of this condition. The continuous version of this expression can be found several references, for instance (Krogstad, 1985) and (Ochi, 1998), and it is applied since it is more convenient from the computational point of view.

$$P\left(net\ ukc_p \leq 0\right) = \left\{1 - \prod_{i=1}^{n}\left[1 - P\left(net\ ukc_{i,p} \leq 0\right)\right]^{\frac{\Delta t_i}{T_{zi,p}}}\right\} \qquad (25)$$

The acceptance criteria for a soft bottom seabed is defined as: the net underkeel clearance shall be at least 0.5m for the average predicted environmental condition; the maximum bottom probability must be less than 10^{-2}; the average probability of bottom touch must be less than 10^{-4}; the maneuverability margin (without wave motions) shall be satisfied in all sections.

In the real time mode the “GO” or “DO NOT GO” decision is performed based on the environmental condition parameters. If these parameters are in the range of the allowance curves presented earlier the decision is “GO”. If they are not, the maneuver is postponed to guarantee the safety until the parameters is the pre-established ranges.

Nowadays the cloud computing provides a large computational capacity and the data transfer of the monitoring system is very robust, as the internet access in several platforms. The measured metocean data (from wave buoys, tide gauge, anemometer and adcp) are downloaded from a specific ftp and the

maneuvering information are provided by the pilot's datacenter using a standard "xml" format. The computations are performed in the cloud and the outputs format and platform may be customized according to the user preferences, as illustrated in Figure 25. Since different users may require different data, a single database is managed in the cloud to provide each user with the required information. The underkeel clearance computation, best predicted window and metocean data is available for all users with different levels of complexity (e.g: directional sea spectrum data, two partition sea spectrum or single partition information).

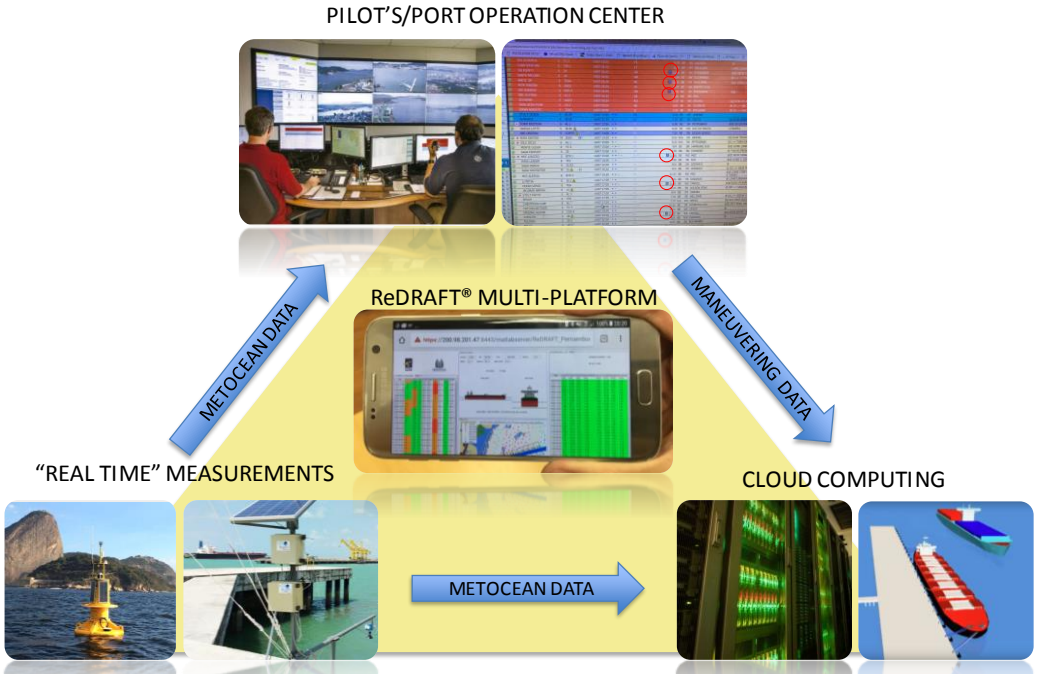

Figure 25 – ReDRAFT® integration of metocean data and maneuver list.

RESULTS AND CONCLUSIONS

The system has been operational since 2015 in Santos Port, the largest one in Latin America with 62 berths and it receives vessels with draft up to 14.2m under favorable environmental conditions. A total of approximately 5000 ships are maneuvered in the port annually. The port is located in São Paulo state and is responsible for almost 30% of the international trades in goods, being, therefore, very important for the country economics. The system was developed in partnership with the Numerical Offshore Tank (TPN) of University of São Paulo and Santos Pilots Association in order to provide more safety and efficiency to the port due to the increase of maneuvers with larger vessels, specially the 336m container ship class. Besides the port is located inside a bay with a huge siltation rate, which may achieve up to 10 cm/month in some parts of the access channel if no maintenance dredging is performed.

The results of 515 critical maneuvers monitored during the years of 2016/2017 are presented in Figure 26, where the blue bars represent cases where the dynamic draft is larger than the static one, providing more efficiency in terms of waiting time. On the other hand, the red bars represent cases where the static rule is not enough to provide navigation safety and a reduction in ship draft is proposed. It can be verified that the ReDRAFT® system can increase both efficiency and safety of the port, which could be also verified based on the downtime of the port due to draft restrictions, which was reduced in almost 50% comparing the years of 2015 and 2016. The results are even better because during this period the number of maneuvers with larger vessels increased almost 20%.

The system awarded the ANTAQ prize together with Santos Pilots C3OT due to the contribution to navigation safety and efficiency of the port.

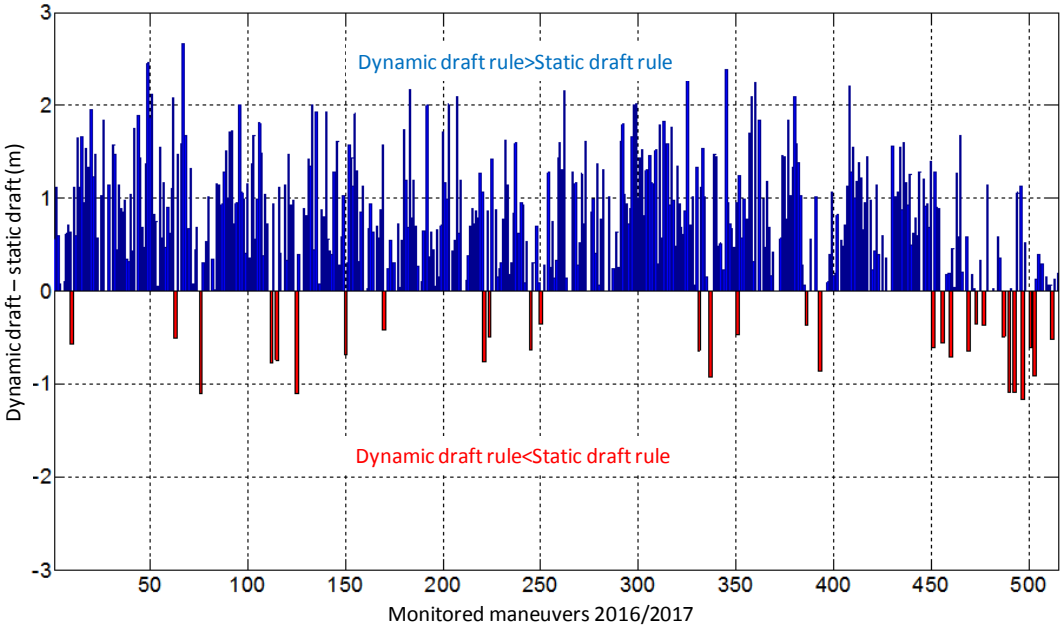

Figure 26 - Comparison of dynamic draft computed by ReDRAFT® and the static draft for critical maneuvers in Santos port.

The system has been extended to Rio de Janeiro Port for containerships, where a validation campaign is being performed together with Rio de Janeiro pilots and containers terminals. The results for 312 observed critical maneuvers can be seen in Figure 27 considering different ship speeds. It can be verified that in some cases a reduction in the draft would be suggested to provide more safety for navigation. However, in most of the cases an increase in ship draft would provide more efficiency without comprising safety.

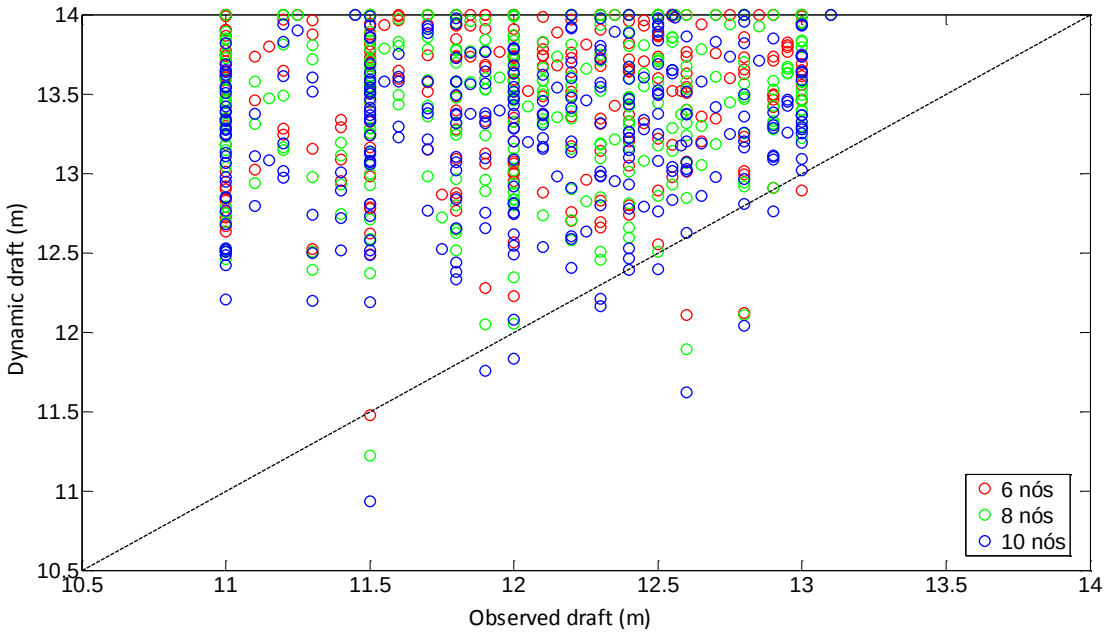

Figure 27 – Comparison of dynamic draft computed by ReDRAFT® and the observed draft for container ship maneuvers in Rio de Janeiro port.

ACKNOWLEDGMENTS

The authors thank the Santos and Rio de Janeiro Pilots for their valuable advices and practical experience during the development. Third and fourth authors thank the National Council for Scientific and Technological Development (CNPq) for the research grant.

REFERENCES

ANTAQ Setor Portuário Nacional. Audiência: Comissão de serviços de infraestrutura. [Relatório]. - Brasilia : [s.n.], 2015.

Bertram Volker Practical Ships Hydrodynamics [Livro]. - 2000.

Blendermann W. Parameter Identification of wind loads on ships [Periódico] // Journal of Wind Engineering and Industrial Aerodynamics. - 1994. - Vol. 51. - pp. 339-351.

Breit S. R. The potential of a Rankine source between parallel planes and in a rectangular channel [Periódico] // Journal of Engineering Mathematics. - 1991. - Vol. 25. - pp. 151-163.

Faltinsen Odd Sea Loads on Ships and Offshore Structures [Livro]. - Cambridge : Cambridge University Press, 1990.

Guha Amitava e Falzarano Jeffrey The effect of small foward speed on prediction of wave loads in restricted water depth [Artigo] // Ocean Systems Engineering. - 2016. - pp. 305-324.

Himeno Y. Prediction of Ship Roll - State of the Art [Relatório]. - Michigan : Dept. of Naval Architecture & Marine Engineering, 1981.

Huuska O. Report Vol 9 - On the Evaluation of Underkeel Clearances in Finnish Waterways [Relatório]. - Helsinki University of Technology. : [s.n.], 1976.

Ikeda Y. [et al.] On Roll Damping Force of Ship. Effects of Hull Surface Pressure Created by Bilge Keels [Periódico] // Journal of the Kansai Society of Naval Architects. - 1977. - Vol. 165. - pp. 31-40.

Ikeda Y. Prediction Method of Roll Damping [Relatório]. - [s.l.] : University of Osaka, 1982.

Ikeda Y., Himeno Y. e Tanaka K. Components of Roll Damping of Ship at Forward Speed [Periódico] // Journal of the Society of Naval Architects. - 1978. - Vol. 143. - pp. 121-133.

Ikeda Y., Himeno Y. e Tanaka K. On Eddy Making Component of Roll Damping Force on Naked Hull [Periódico] // Journal of the Society of Naval Architects. - 1977. - Vol. 142. - pp. 59-69.

Ikeda Y., Himeno Y. e Tanaka N. On Roll Damping Force of Ship. Effects of Frction of Hull and Normal Force of Bilge Keels [Periódico] // Journal of the Kansai Society of Naval Architects. - 1976. - Vol. 161. - pp. 41-49.

IMO - International Maritime Organization GUIDELINES FOR VOLUNTARY USE OF THE SHIP ENERGY EFFICIENCY (EEOI) - MEPC.1/Circ.684 [Relatório]. - London : [s.n.], 2009.

IMO - International Maritime Organization RESOLUTION MSC.267(85) [Relatório]. - 2008.

International Hydrographic Organization IHO Standards for Hydrographic Surveys. - [s.l.] : International Hydrographic Bureau, 2008.

Isherwood R. M. Wind resistance of merchant ships [Periódico] // Transactions of the Royal Institution of Naval Architects. - 1972. - Vol. 114. - pp. 327-338.

John F On the motion of floating bodies I [Periódico] // Pure Applied Mathematics. - 1949. - pp. 13-57.

Journée J. M. J. e Massie W. W. Offshore Hydromechanics [Relatório]. - [s.l.] : Delft University, 2011.

Kristensen H. O. Determination of Regression Formulas for Main Dimensions of Tankers and Bulk Carriers based on IHS Fairplay data [Relatório]. - University of Southern Denmark : [s.n.], 2012.

Kristensen H. O. Statistical Analysis and Determination of Regression Formulas for Main Dimensions of Container Ships based on IHS Fairplay Data [Relatório]. - University of Southern Denmark : [s.n.], 2013.

Krogstad Harald E Height and period distributions of extreme waves [Artigo] // Applied Ocean Research. - 1985. - pp. 158-165.

Lackenby H. On the systematic geometrical variation of ship forms. [Periódico] // Trans. of INA. - 1950. - Vol. 92. - pp. 289-316.

Lewis E. V. Principles of Naval Architecture - Volume III - Motions in Waves and Controllability [Livro]. - 1988.

Li Lin Numerical Seakeeping Predictions of Shallow Water Effect on Two Ship Interactions in Waves. - Halifax : Doctor of Philosophy - Dalhousie University, 2001.

Lindeen C. Wind Resistance Generated by Containers on Reefer Vessels [Livro]. - Stockholm : Master thesis, 2008.

Liu Yingyi, Iwashita Hidetsugu e Hu Changhong A calculation method for finite depth free-surface green function [Artigo] // International Journal of Naval Architecture and Ocean Engineering. - 2015. - pp. 375-389.

Mei Chiang C., Stiassnie M. e Yue Dick K.-P. Theory and applications of ocean surface waves. Part 1: Linear Aspects [Livro]. - [s.l.] : World Scientific, 2005.

Newman J. N. Algorithms for the free surface Green function [Artigo] // Journal of Engineering Mathematics. - 1985. - pp. 57-67.

Newman John Nicholas Marine Hydrodynamics [Livro]. - [s.l.] : MIT Press, 1977.

Newman John Nicholas The Green function for potential flow in a rectangular channel [Periódico] // Journal of Engineering Mathematics. - 1992. - Vol. 26. - pp. 51-59.

Ochi Michel K. Ocean Waves: the stochastic approach [Relatório]. - [s.l.] : Cambridge University Press, 1998.

PIANC Report n. 121 - Harbour Approach Channels Design Guidelines [Relatório]. - [s.l.] : The World Association for Waterborne Transport Infrastructure, 2014.

PIANC Report nº121 - Harbour Approach Channels Design Guidelines [Relatório]. - Bruxelles : [s.n.], 2014.

PIANC Underkeel clearance for Large Ships in Maritime Fairways with hard bottom (Bulletin Nº51). - Bruxelas : [s.n.], 1985.

Ruggeri F. [et al.] On the development of a higher order time-domain Rankine panel method for linear and weakly non-linear seakeeping computations [Periódico] // Journal of the Brazilian Society of Mechanical Sciences and Engineering. - 2018. - Vol. 40. - p. 70.

Ruggeri F. A Higher Order Time Domain Panel Method for Linear and Weakly Non Linear Seakeeping Problems.. - São Paulo : [s.n.], 2016.

Ruggeri F. A Time Domain Rankine Panel Method for 2D Seakeeping Analysis. - São Paulo : [s.n.], 2012.

Schneekluth H. e Bertram V. Ship Design for Efficiency & Economy [Livro]. - 1998.

Tannuri E. A. [et al.] Modular Mathematical Model for a Low-Speed Maneuvering Simulator [Artigo] // Proceedings of the ASME 2014 33rd International Conference on Ocean, Offshore and Arctic Engineering. - 8-13 de June de 2014.

WAMIT Inc WAMIT USER MANUAL 7.2 [Relatório]. - 2015.

Wehausen John V e Laitone Edmund V Surface Waves in Fluid Dynamics III [Seção do Livro]. - 1960.

Yamano T. e Saito Y. An Estimation Method of Wind Force Acting on Ship's Hull [Artigo] // Journal of Kansai Society of Naval Architects. - 1197.

Yilmaz H. e Guner M. An Approximate Method for Cross Curves of Cargo Vessels [Livro]. - 2001.